Enhanced spin Hall effect of light scattering on a meta-atom with bianisotropy

Wenjia Li [1,2] Jianlong Liu,[2,*] Yang Gao,[3] Keya Zhou,[1] and Shutian Liu[1,†]
[1]*School of Physics, Harbin Institute of Technology, Harbin 150001, China*
[2]*Key Laboratory of In-Fiber Integrated Optics of Ministry of Education, College of Physics and Optoelectronic Engineering, Harbin Engineering University, Harbin 150001, China*
[3]*College of Electronic Engineering, Heilongjiang University, Harbin 150080, China*

(Received 4 March 2020; accepted 8 December 2020; published 22 December 2020)

We reveal an interesting phenomenon of enhanced polarization-dependent transverse deflection of scattered light on a meta-atom with bianisotropy. The relationship between the spin-dependent shift and the bianisotropy is demonstrated. Unlike the usual particle, the obvious transverse scattering can be obtained by the bianisotropy. Furthermore, the lateral optical force exerted on the bianisotropic meta-atom is inevitable due to the spin Hall effect of light. This work provides a way to achieve an enhanced spin Hall effect of light and offers a platform to study the interaction between light and meta-atom with bianisotropy.

DOI: 10.1103/PhysRevA.102.063527

I. INTRODUCTION

Light can carry spin angular momentum (SAM) and orbital angular momentum (OAM). SAM depends on the polarization state of light. OAM can be split into intrinsic orbital angular momentum (IOAM) and extrinsic orbital angular momentum (EOAM), which are determined by the field spatial phase distribution and the propagation path. Spin-orbit interaction (SOI) is the interaction between SAM and OAM of light, which has attracted considerable attention in metasurface [1–6], crystals [7–9], waveguides [10–15], and so on. The spin Hall effect (SHE) of light refers to the procedure where the SAM of light couples to the EOAM of the output light. The SHE has numerous potential applications, which may be conducive to the further development of precision metrology and spin-optics devices [16–20]. Therefore, how to enhance the SHE has become a key issue in its applications.

In the last decade there have been growing interest in the enhanced SHE of light [21–29]. Several methods were proposed, such as topologically protected edge states [24], structured metamaterial [22], plasmon resonance [25], and so on. For nanoparticles, enhancing the SHE has also received great interest in recent years [27–29]. It has been reported that giant SHE for a spherical nanoparticle can be realized by judiciously displacing the scatterer in the focal volume [27]. The far field of the scattered light with opposite helicity is split into two opposite sides. An enhanced SHE on dielectric spheres with dual symmetry has been demonstrated, which originates from the strong SOI of light in the near field [28]. The other method to enhance the SHE has been proposed by using core-shell nanoparticles [29]. These two works all focus on the transverse shift in the perceived location of the radiation. In our previous work we investigated the SHE on an ellipsoidal Rayleigh particle in scattered light [30]. When the light incidence is inclined to the main axis of ellipsoidal Rayleigh particle, such a shift of the barycenter of the scattered light is unavoidable. Due to the weak anisotropy of the ellipsoidal particle, the phenomenon of SHE on it is not so obvious. Recently, the photonic SHE mediated by bianisotropy has been demonstrated by using polarization-dependent routing of linearly polarized (LP) light [31]. The SHE is provided by two LP incidences with symmetric polarization directions, which results in asymmetric scattering. Here we give the relationship between the barycenter of scattered light and the circularly polarized incidence, and make a connection between the SHE and the lateral optical force.

In this paper we propose an enhanced SHE of light scattering on a meta-atom with bianisotropy. We give detailed analytical expressions to describe the relationship between the barycenter of the scattered light and the spin state of the incident light in theory and simulation. The tunable SHE can be obtained by changing the incident angle and the size of the meta-atom. The transverse scattering is quite apparent owing to the bianisotropic response. Compared with the previous work [30], the maximum transverse angle shift for the intensity barycenter of the scattered light is enhanced by three orders of magnitude. Besides, we reveal that the lateral optical force is generated by the interaction between the light and the meta-atom. The results are conducive to the further development of precision metrology, spin-based photonic devices, and optical driven micromachines.

II. THEORY MODEL

We consider a meta-atom with bianisotropy illuminated by left or right circularly polarized (LCP or RCP) light as shown in Fig. 1. The meta-atom with bianisotropy consists of two ceramic disks with diameters (d_1, d_2), and heights (h_1, h_2). The surrounding medium is a free space. We assume that the meta-atom with bianisotropy has electric and magnetic dipole responses without higher order multipoles. In the following we employ the CGS system of units. The electric and mag-

*liujl@hit.edu.cn
†stliu@hit.edu.cn

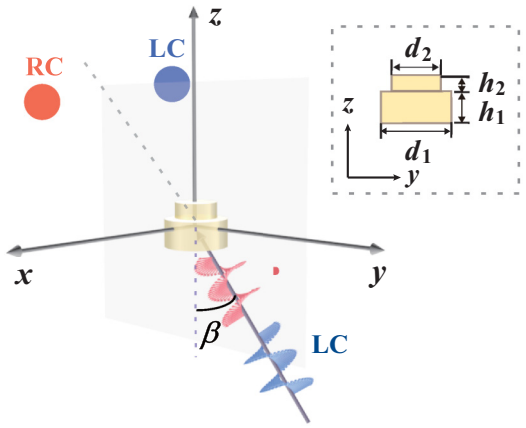

FIG. 1. Illustration of spin Hall effect of scattered light from a meta-atom with bianisotropy. The red and blue rotatory arrows represent the incident RCP and LCP light, respectively. The incident angle β is the angle between the incident light and the z axis in the y-z plane. The output red and blue circles represent the intensity barycenters of the scattered light for the incident RCP and LCP light, respectively. The inset shows the geometric view of the meta-atom with bianisotropy, which consists of two ceramic disks with diameters (d_1, d_2) and heights (h_1, h_2).

netic dipole moments of the meta-atom with bianisotropy can be described as [31]

$$\mathbf{p} = \overline{\alpha}_{\mathrm{ee}} \cdot \mathbf{E}_{\mathrm{i}} + \overline{\alpha}_{\mathrm{em}} \cdot \mathbf{H}_{\mathrm{i}}, \tag{1}$$

$$\mathbf{m} = \overline{\alpha}_{\mathrm{me}} \cdot \mathbf{E}_{\mathrm{i}} + \overline{\alpha}_{\mathrm{mm}} \cdot \mathbf{H}_{\mathrm{i}}, \tag{2}$$

where $\mathbf{E}_{\mathrm{i}}$ and $\mathbf{H}_{\mathrm{i}}$ are the incident electric and magnetic fields, and $\overline{\alpha}_{\mathrm{ee}}$, $\overline{\alpha}_{\mathrm{em}}$, $\overline{\alpha}_{\mathrm{me}}$, and $\overline{\alpha}_{\mathrm{mm}}$ denote 3×3 polarizability tensors. Considering the meta-atom with bianisotropy, the polarizability tensors can be expressed as

$$\overline{\alpha}_{\mathrm{ee}} = \begin{pmatrix} \alpha_{\mathrm{ee}}^{xx} & 0 & 0 \\ 0 & \alpha_{\mathrm{ee}}^{xx} & 0 \\ 0 & 0 & \alpha_{\mathrm{ee}}^{zz} \end{pmatrix}, \tag{3}$$

$$\overline{\alpha}_{\mathrm{mm}} = \begin{pmatrix} \alpha_{\mathrm{mm}}^{xx} & 0 & 0 \\ 0 & \alpha_{\mathrm{mm}}^{xx} & 0 \\ 0 & 0 & \alpha_{\mathrm{mm}}^{zz} \end{pmatrix}, \tag{4}$$

$$\overline{\alpha}_{\mathrm{em}} = \overline{\alpha}_{\mathrm{me}} = \begin{pmatrix} 0 & i\gamma & 0 \\ -i\gamma & 0 & 0 \\ 0 & 0 & 0 \end{pmatrix}. \tag{5}$$

The input light field is obliquely incident on the meta-atom and the incident angle β is the angle between the incident light and the z axis. The incidence is in the y-z plane. The oblique input light field can be written as

$$\mathbf{E}_{\mathrm{i}} = \mathrm{E}_0(-\sigma i\hat{\mathbf{x}} + \cos\beta\hat{\mathbf{y}} + \sin\beta\hat{\mathbf{z}})e^{ik_0(-\sin\beta y + \cos\beta z)}, \tag{6}$$

$$\mathbf{H}_{\mathrm{i}} = \mathrm{H}_0(-\hat{\mathbf{x}} - \sigma i\cos\beta\hat{\mathbf{y}} - \sigma i\sin\beta\hat{\mathbf{z}})e^{ik_0(-\sin\beta y + \cos\beta z)}, \tag{7}$$

where k_0 is the wave number in vacuum, σ denotes the helicity of the beam, and $\mathrm{E}_0 = \mathrm{H}_0$ are the amplitudes of incident electric and magnetic fields. The helicity is chosen as $\sigma \equiv 0$, 1, and -1 corresponding to the LP, RCP, and LCP, respectively. The far field scattered by the meta-atom is given by [32,33]

$$\mathbf{E}_{\mathrm{s}} = \frac{k_0^2 e^{ik_0 r}}{r}[(\hat{\mathbf{n}} \times \mathbf{p}) \times \hat{\mathbf{n}} - \hat{\mathbf{n}} \times \mathbf{m}], \tag{8}$$

$$\mathbf{H}_{\mathrm{s}} = \hat{\mathbf{n}} \times \mathbf{E}_{\mathrm{s}}, \tag{9}$$

where r is the distance away from the scatterer and $\hat{\mathbf{n}}$ is the unit direction vector. In vacuum, the time-averaged intensity of the scattered light for a monochromatic electromagnetic beam can be expressed as

$$\langle \mathbf{S} \rangle = \tfrac{1}{2}\mathrm{Re}(\mathbf{E}_{\mathrm{s}} \times \mathbf{H}_{\mathrm{s}}^*). \tag{10}$$

In this paper we investigate the SHE by the intensity barycenter of the scattered light. In the spherical coordinate system, the position of the intensity barycenter of the scattered light can be described by the cosine functions of the azimuthal angle (φ) and the elevation angle (θ) as [30,34]

$$\langle \cos\varphi \rangle = \frac{\iint \cos\varphi S_r r^2 \sin\theta d\theta d\varphi}{\iint S_r r^2 \sin\theta d\theta d\varphi}, \tag{11}$$

$$\langle \cos\theta \rangle = \frac{\iint \cos\theta S_r r^2 \sin\theta d\theta d\varphi}{\iint S_r r^2 \sin\theta d\theta d\varphi}, \tag{12}$$

where S_r is the radial component of the time-averaged intensity of the scattered light. After some derivations we obtain

$$\langle \cos\varphi \rangle = \frac{3\pi}{16}\sigma \sin\beta \frac{C_2\cos\beta + C_3}{C_1}, \tag{13}$$

$$\langle \cos\theta \rangle = \frac{C_4\cos\beta + C_5}{2C_1}, \tag{14}$$

with

$$\begin{aligned} C_1 = \mathrm{Re}\big[&\alpha_{\mathrm{ee}}^{xx2}(\cos^2\beta + \sigma^2) + \alpha_{\mathrm{ee}}^{zz2}\sin^2\beta \\ &+ \alpha_{\mathrm{mm}}^{xx\ 2}(\sigma^2\cos^2\beta + 1) + \sigma^2\alpha_{\mathrm{mm}}^{zz\ 2}\sin^2\beta \\ &+ \gamma^2(\cos^2\beta + \sigma^2 + \sigma^2\cos^2\beta + 1) \\ &+ i(\sigma^2 + 1)\big(\alpha_{\mathrm{ee}}^{xx*}\gamma - \alpha_{\mathrm{ee}}^{xx}\gamma^*\big)\cos\beta \\ &+ i(\sigma^2 + 1)\big(\alpha_{\mathrm{mm}}^{xx}\gamma^* - \alpha_{\mathrm{mm}}^{xx\ *}\gamma\big)\cos\beta\big], \end{aligned} \tag{15}$$

$$\begin{aligned} C_2 = \mathrm{Re}\big[&i\big(\alpha_{\mathrm{mm}}^{xx}\alpha_{\mathrm{ee}}^{zz*} - \alpha_{\mathrm{mm}}^{xx\ *}\alpha_{\mathrm{ee}}^{zz}\big) \\ &+ i\big(\alpha_{\mathrm{mm}}^{zz\ *}\alpha_{\mathrm{ee}}^{xx} - \alpha_{\mathrm{mm}}^{zz}\alpha_{\mathrm{ee}}^{xx*}\big)\big], \end{aligned} \tag{16}$$

$$C_3 = \mathrm{Re}\big[\big(\alpha_{\mathrm{ee}}^{zz*}\gamma + \alpha_{\mathrm{ee}}^{zz}\gamma^*\big) - \big(\alpha_{\mathrm{mm}}^{zz\ *}\gamma + \alpha_{\mathrm{mm}}^{zz}\gamma^*\big)\big], \tag{17}$$

$$C_4 = \mathrm{Re}\big[\big(\alpha_{\mathrm{mm}}^{xx}\alpha_{\mathrm{ee}}^{xx*} + \alpha_{\mathrm{mm}}^{xx\ *}\alpha_{\mathrm{ee}}^{xx} - 2\gamma^2\big)(1 + \sigma^2)\big], \tag{18}$$

$$\begin{aligned} C_5 = \mathrm{Re}\big[&i\big(\alpha_{\mathrm{ee}}^{xx}\gamma^* - \alpha_{\mathrm{ee}}^{xx*}\gamma\big)(\cos^2\beta + \sigma^2) \\ &+ i\big(\alpha_{\mathrm{mm}}^{xx\ *}\gamma - \alpha_{\mathrm{mm}}^{xx}\gamma^*\big)(\sigma^2\cos^2\beta + 1)\big]. \end{aligned} \tag{19}$$

It indicates that the cosine functions of the azimuthal angle are reverse and the cosine functions of the elevation angle are the same for the incident RCP and LCP light. According to Eqs. (13) and (14) we can deduce that the positions of the intensity barycenters of the scattered light for the incident RCP

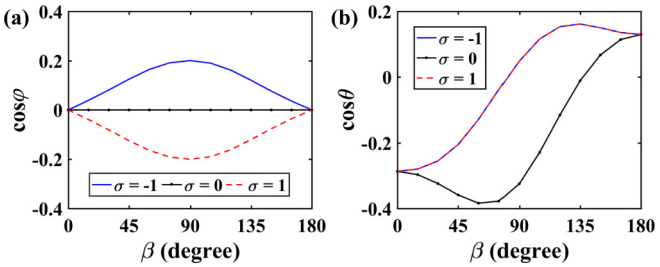

FIG. 2. (a) Changes in the cosine values of the azimuthal angles for the barycenter of the scattered light with the incident angle. (b) Changes in the cosine values of the elevation angles for the barycenter of the scattered light with the incident angle. The frequency of the incident light is 2.5 GHz. The diameters of the bianisotropic meta-atom are $d_1 = 29.1$ mm and $d_2 = 17.5$ mm. The heights of the bianisotropic meta-atom are $h_1 = 9.0$ mm and $h_2 = 3.0$ mm.

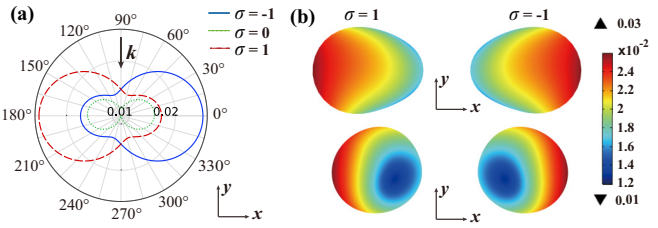

FIG. 3. (a) Two-dimensional scattering diagram of the meta-atom with bianisotropy in *Oxy* plane for the incident LCP, LP, and RCP light. The direction of the incident light is along the negative y axis. The blue, green, and red lines represent the scattering patterns of the incident LCP, LP, and RCP light, respectively. (b) Three-dimensional scattering diagrams of the meta-atom with bianisotropy in *Oxy* and *Oxz* planes. The legend shows the magnitude of the scattered electric field.

and LCP light are symmetric about the plane of incidence unless the incident angle is 0° or 180°, and the phenomenon is a typical SHE of scattered light. Compared with our previous work [30], the cosine functions of the azimuthal and elevation angles are more complex due to the cross coupling in a meta-atom with bianisotropy. It is worth noting that the symmetric spin split can occur when the incident light is along negative y axis ($\beta = 90°$), which originates from the broken mirror symmetry.

III. RESULTS AND DISCUSSIONS

To verify the predictions of our theoretical analysis, we give some examples and simulation results obtained by the commercial software COMSOL Multiphysics. In the simulation the meta-atom with bianisotropy consists of two ceramic disks [31] and the relative permittivity of ceramic is 39. The diameters of the two disks are $d_1 = 29.1$ mm and $d_2 = 17.5$ mm. The heights of the two disks are $h_1 = 9.0$ mm and $h_2 = 3.0$ mm. The frequency of the incident light is 2.5 GHz. First, we investigate the changes in the cosine values of the azimuthal angles for the barycenter of the scattered light with the incident angle as shown in Fig. 2(a). It can be seen that the cosine values of the azimuthal angles for the incident LCP and RCP light are opposite to each other unless the incident angle is 0° or 180°, which is in accordance with the theory. Besides, the cosine values of the azimuthal angles can be maximized when the incident angle is 90° in this case. The cosine value of the azimuthal angle is much bigger than previous reported results [30]. The bigger cosine values of the azimuthal angles respond to a stronger SHE of the scattered light. Second, the changes in the cosine values of the elevation angles for the barycenter of the scattered light with the incident angle is shown in Fig. 2(b). It is found that the cosine values of the elevation angles for the incident LCP and RCP light are the same, which agrees well with our theory. The intensity barycenters of the scattered light for RCP and LCP are symmetric about the plane of incidence, which is a typical polarization-dependent split.

Figure 3(a) depicts the two-dimensional scattering diagram of the meta-atom with bianisotropy in *Oxy* plane for the incident LCP, LP, and RCP light along the negative y axis ($\beta = 90°$). We notice that there are clear symmetric transverse scatterings for the incident LCP and RCP light. Such effects are realized owing to the interference between the waves radiated by the electric and magnetic dipole moments of the bianisotropic meta-atom. The corresponding three-dimensional scattering patterns in *Oxy* and *Oxz* planes are shown in Fig. 3(b).

It is clear that the scattered light for RCP and LCP are symmetric about the plane of incidence and the SHE of the scattered light is quite remarkable. It provides a very efficient way to obtain the spin-split scattering. Moreover, the transverse scattering of nanostructures is of great importance in various nanophotonic applications, such as efficient beam control, precision metrology, and spin-based photonic devices.

To explore the intrinsic properties which are linked to the scattering, we calculated the polarizability tensors of the meta-atom using the method proposed in Ref. [35]. Figure 4 shows the changes in the real and imaginary parts of the different

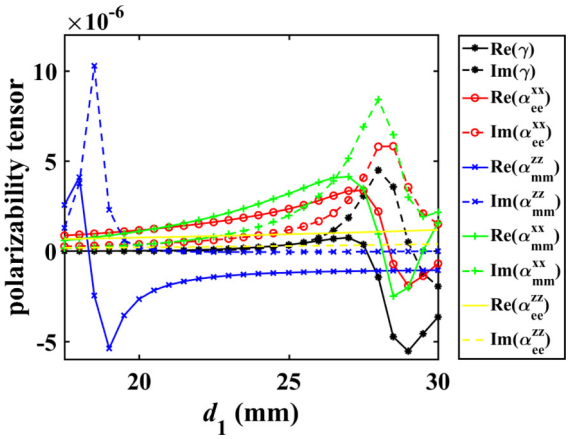

FIG. 4. (a) Changes in the real and imaginary parts of the different polarizability tensors with the diameter d_1 from 17.5 to 30 mm. The frequency of the incident light is 2.5 GHz. The other diameter of the bianisotropic meta-atom is $d_2 = 17.5$ mm. The heights of the bianisotropic meta-atom are $h_1 = 9.0$ mm and $h_2 = 3.0$ mm, respectively.

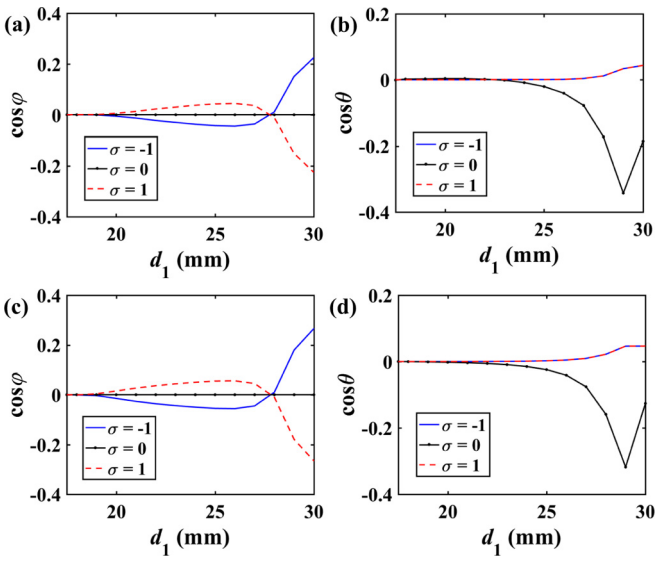

FIG. 5. (a) and (b) Dependencies of the cosine values of azimuthal and elevation angles for the barycenter of the scattered light on diameter d_1 by the dipole model. (c) and (d) Dependencies of the cosine values of azimuthal and elevation angles for the barycenter of the scattered light on diameter d_1 in simulation.

polarizability tensors with the disk diameter d_1. The real line represents the real part, and the dotted line represents the imaginary part. The different colors correspond to different polarizability tensors. The frequency of the incident light is 2.5 GHz. The other diameter of the bianisotropic meta-atom is $d_2 = 17.5$ mm. The heights of the bianisotropic meta-atom are $h_1 = 9.0$ mm and $h_2 = 3.0$ mm, respectively. It shows that the electromagnetic coupling coefficient γ exhibits a comparable strength with the electric and magnetic polarizabilities at some frequencies. There are also two clear resonances in z (in blue) and $x(y)$ (in other colors) directions. It can be predicted that the change of the polarizability tensor will have significant influence on the SHE of light, especially at the position of the resonance.

In order to get a bigger spin-dependent transverse shift, we choose the incident light along the negative y axis in the following discussion. The resulting polarizability tensors are substituted into Eqs. (13) and (14) to get the cosine values of azimuthal and elevation angles for the barycenter of the scattered light. The results are shown in Figs. 5(a) and 5(b). It is clear that the cosine values of the azimuthal angles are reversed and the cosine values of elevation angles are the same for the incident LCP and RCP light except for $d_1 = d_2$. At $d_1 = d_2$ (17.5 mm), the spin-dependent transverse shift disappears due to the absent bianisotropy for the meta-atom, which suggests that the obtained conditions in Eq. (13) hold. The direction of the lateral shift [shown in Fig. 5(a)] is reversed around $d_1 = 28$ mm due to the change of the polarizability tensors. As shown in Fig. 4, there is an obvious resonance and a sharp change in the coupling coefficient. In Figs. 5(c) and 5(d) we show the simulation results of the barycenter of the scattered light with the same parameters. Compared with Figs. 5(a) and 5(b), it is found that there is a good agreement between them, which proves the accuracy of our theory. The SHE by the meta-atom highly depends on the shape and the size of the structure. In order to obtain an enhanced SHE, we need to carefully adjust the structure and size of the meta-atom to satisfy the particular relationship described by Eqs. (13) and (14). The enhanced SHE proposed in this work can be easily demonstrated in experiments. The bianisotropic meta-atom is made of two coaxial ceramic disks. One can utilize a microwave network analyzer to measure the scattered field of the meta-atom. An angle sweep can be carried out to get a full-angle intensity distribution around the meta-atom. Then, the barycenter of the scattered light can be obtained using Eqs. (11) and (12).

The SHE of light not only manifests in the far field but could also exists in the near field. Considering the interaction between the particle and some kind of supporting surface [36–38], the study may be more practical. It is believed that the SHE of light could still exist when the particle interacts with surfaces. But the particle-surface interactions will influence the effect. In addition, the SHE of light could exist in near field arising from the interaction between surface plasmon or phonon polaritons and the bianisotropic particle.

IV. LATERAL OPTICAL FORCE

To thoroughly understand the interaction between the scattered light and the meta-atom with bianisotropy, we calculate the optical force exerted on the meta-atom by integrating the Maxwell stress tensor over a surface S enclosing the

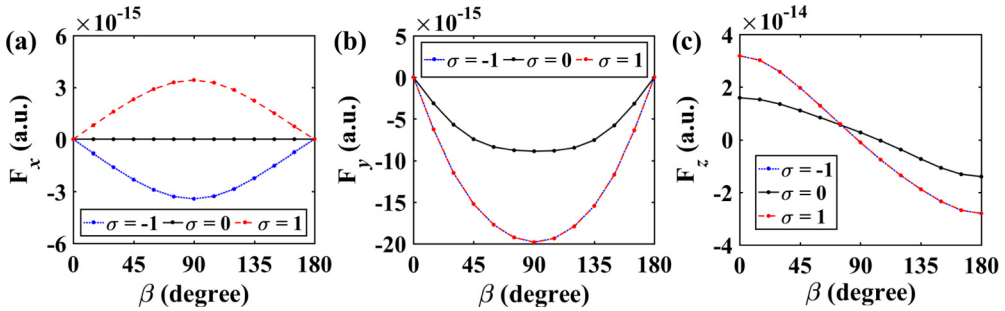

FIG. 6. (a)–(c) Changes in the x, y, and z components of optical forces with different incident angles. The frequency of the incident light is 2.5 GHz. The diameters of the bianisotropic meta-atom are $d_1 = 29.1$ mm and $d_2 = 17.5$ mm. The heights of the bianisotropic meta-atom are $h_1 = 9.0$ mm and $h_2 = 3.0$ mm.

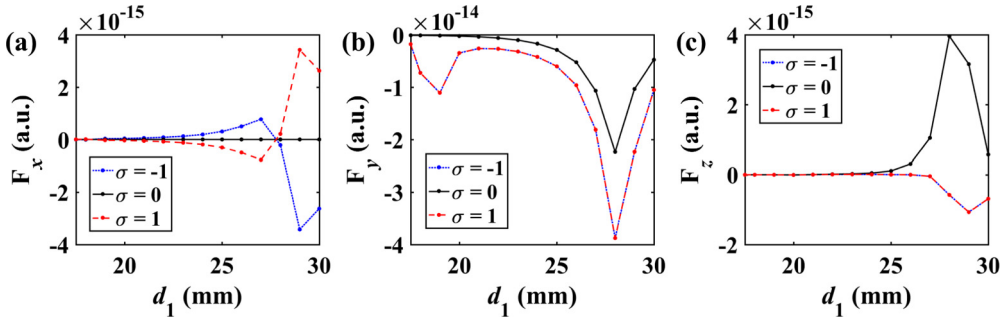

FIG. 7. (a)–(c) Changes in the x, y, and z components of the optical forces with diameter d_1, respectively. The frequency of the incident light is 2.5 GHz and the incident angle is 90°. The other diameter of the bianisotropic meta-atom is $d_2 = 17.5$ mm. The heights of the bianisotropic meta-atom are $h_1 = 9.0$ mm and $h_2 = 3.0$ mm.

meta-atom that can be written as

$$\langle \mathbf{F} \rangle = \oint_S \hat{\mathbf{n}} \cdot \langle \overline{\mathbf{T}} \rangle dS, \tag{20}$$

where $\hat{\mathbf{n}}$ is the unit outward normal vector and $\langle \overline{\mathbf{T}} \rangle$ is the time-averaged Maxwell stress tensor can be expressed as

$$\langle \overline{\mathbf{T}} \rangle = \tfrac{1}{2}\mathrm{Re}\big[\epsilon \mathbf{E}\mathbf{E}^* + \mu \mathbf{H}\mathbf{H}^* - \tfrac{1}{2}(\epsilon \mathbf{E}\cdot\mathbf{E}^* + \mu \mathbf{H}\cdot\mathbf{H}^*)\overline{\mathbf{I}}\big], \tag{21}$$

with $\overline{\mathbf{I}}$ is the unit tensor, and ϵ and μ are the permittivity and permeability of the surrounding medium, respectively. The transverse shift of the barycenter of the scattered light corresponds to a lateral optical force as a result of the interaction between light and matter. Figures 6(a)–6(c) illustrate the changes in the x, y, and z components of optical force with the incident angle. The x components of optical forces are opposite to each other for the incident LCP and RCP light, as illustrated in Fig. 6(a). However, the y and z components of optical force are irrelevant to the handedness of the incident light. The phenomenon is unavoidable and consistent with the SHE of the scattered light. The barycenters of the scattered light for the RCP and LCP incidences are symmetric about the plane of incidence (y-z plane), so the x components of optical forces exerted on the meta-atom for the incident RCP and LCP light are reversed inevitably.

The dependence of the x, y, and z components of the optical force on diameter d_1 are depicted in Figs. 7(a)–7(c). It is easy to observe that the handedness of the incident light influences the x component of the optical force but not the y and z components. As it has been demonstrated, the change of the optical force is synchronous with the change of the barycenter of the scattered light. The direction of the x component of the optical force is reversed around $d_1 = 28$ mm in Fig. 7(a), which coincides with Figs. 5(a) and 5(c). The optical force is a manifestation of the SHE of the scattered light and is conducive to understand the interaction between light and the meta-atom with bianisotropy. It suggests that the lateral optical force can be controlled by the spin state of the incident light, which may provide a useful toolset for optical manipulation of the meta-atom. Although we only consider the standalone particle in this paper, it is believed that the lateral optical force acting on the meta-atom still exists when it is placed above a substrate [39]. The lateral optical forces exerted on particles can also be achieved by other nanophotonic structures such as hyperbolic and extremely anisotropic metasurfaces [40].

V. CONCLUSION

We demonstrate an enhanced SHE on a meta-atom with bianisotropy. Based on the dipole model, we present the detailed analytical expressions to describe the relationship between the barycenter of the scattered light and the spin state of light. It is found that the barycenter of the scattered light is highly dependent on the polarization state of the incident light, which results in an enhanced SHE. The influence of the incident angle of light, and the size of the meta-atom, on the direction of the barycenter of the scattered light have been presented. The maximum angle shift of the intensity barycenter is obviously enhanced compared with previous works. Moreover, we reveal the interaction between helical light and the meta-atom by analyzing the optical force. The transverse shift of the scattered light corresponds to the lateral optical force exerted on the meta-atom. We believe that unveiling such a phenomenon is promising for related technologies of precision metrology, spin-based photonic devices, and optical driven micromachines.

ACKNOWLEDGMENTS

This work was supported by the National Basic Research Program of China under Grant No. 2013CBA01702, and the National Natural Science Foundation of China under Grants No. 61575055, No. 11874132, No. 61405056, and No. 12074087.

[1] X. Yin, Z. Ye, J. Rho, Y. Wang, and X. Zhang, Science **339**, 1405 (2013).

[2] N. Shitrit, I. Bretner, Y. Gorodetski, V. Kleiner, and E. Hasman, Nano Lett. **11**, 2038 (2011).

[3] N. Shitrit, I. Yulevich, E. Maguid, D. Ozeri, D. Veksler, V. Kleiner, and E. Hasman, Science **340**, 724 (2013).

[4] J. Lin, J. B. Mueller, Q. Wang, G. Yuan, N. Antoniou, X.-C. Yuan, and F. Capasso, Science **340**, 331 (2013).

[5] K. Y. Bliokh, Y. Gorodetski, V. Kleiner, and E. Hasman, Phys. Rev. Lett. **101**, 030404 (2008).

[6] L. Jing, Z. Wang, Y. Yang, L. Shen, B. Zheng, F. Gao, H. Wang, E. Li, and H. Chen, IEEE T. Antenn. Propag. **66**, 7148 (2018).

[7] E. Brasselet, Y. Izdebskaya, V. Shvedov, A. S. Desyatnikov, W. Krolikowski, and Y. S. Kivshar, Opt. Lett. **34**, 1021 (2009).

[8] X. Lu and L. Chen, Opt. Express **20**, 11753 (2012).

[9] M. Liu, L. Cai, S. Chen, Y. Liu, H. Luo, and S. Wen, Phys. Rev. A **95**, 063827 (2017).

[10] J. Petersen, J. Volz, and A. Rauschenbeutel, Science **346**, 67 (2014).

[11] Y. Liang, H. W. Wu, B. J. Huang, and X. G. Huang, Nanoscale **6**, 12360 (2014).

[12] W. Li, J. Liu, Y. Gao, K. Zhou, and S. Liu, J. Phys. D: Appl. Phys. **52**, 195103 (2019).

[13] W. Li, J. Liu, Y. Gao, K. Zhou, and S. Liu, Opt. Express **27**, 10208 (2019).

[14] W. Li, J. Liu, Y. Gao, K. Zhou, and S. Liu, J. Phys. D: Appl. Phys. **53**, 025110 (2020).

[15] Y. Liang, F. Zhang, J. Gu, X. G. Huang, and S. Liu, Sci. Rep. **6**, 24959 (2016).

[16] X. Zhou, X. Ling, H. Luo, and S. Wen, Appl. Phys. Lett. **101**, 251602 (2012).

[17] X. Zhou, Z. Xiao, H. Luo, and S. Wen, Phys. Rev. A **85**, 043809 (2012).

[18] X. Zhou, L. Sheng, and X. Ling, Sci. Rep. **8**, 1221 (2018).

[19] G. Araneda, S. Walser, Y. Colombe, D. B. Higginbottom, J. Volz, R. Blatt, and A. Rauschenbeutel, Nat. Phys. **15**, 17 (2019).

[20] T. Zhu, Y. Lou, Y. Zhou, J. Zhang, J. Huang, Y. Li, H. Luo, S. Wen, S. Zhu, Q. Gong *et al.*, Phys. Rev. Appl. **11**, 034043 (2019).

[21] H. Luo, X. Zhou, W. Shu, S. Wen, and D. Fan, Phys. Rev. A **84**, 043806 (2011).

[22] X. Ling, X. Zhou, X. Yi, W. Shu, Y. Liu, S. Chen, H. Luo, S. Wen, and D. Fan, Light Sci. Appl. **4**, e290 (2015).

[23] X.-H. Ling, H.-L. Luo, M. Tang, and S.-C. Wen, Chin. Phys. Lett. **29**, 074209 (2012).

[24] A. P. Slobozhanyuk, A. N. Poddubny, I. S. Sinev, A. K. Samusev, Y. F. Yu, A. I. Kuznetsov, A. E. Miroshnichenko, and Y. S. Kivshar, Laser Photonics Rev. **10**, 656 (2016).

[25] Y. Xiang, X. Jiang, Q. You, J. Guo, and X. Dai, Photonics Res. **5**, 467 (2017).

[26] L.-J. Kong, S.-X. Qian, Z.-C. Ren, X.-L. Wang, H.-T. Wang *et al.*, Phys. Rev. A **85**, 035804 (2012).

[27] M. Neugebauer, S. Nechayev, M. Vorndran, G. Leuchs, and P. Banzer, Nano Lett. **19**, 422 (2018).

[28] D. Gao, R. Shi, A. E. Miroshnichenko, and L. Gao, Laser Photonics Rev. **12**, 1800130 (2018).

[29] R. Shi, D. L. Gao, H. Hu, Y. Wang, and L. Gao, Opt. Express **27**, 4808 (2019).

[30] W. Li, J. Liu, Y. Gao, K. Zhou, and S. Liu, Opt. Express **27**, 28194 (2019).

[31] D. V. Zhirihin, S. V. Li, D. Y. Sokolov, A. P. Slobozhanyuk, M. A. Gorlach, and A. B. Khanikaev, Opt. Lett. **44**, 1694 (2019).

[32] J. D. Jackson, *Classical Electrodynamics* (Wiley, New York, 2001).

[33] L. D. Landau and E. M. Lifshitz, *Course of Theoretical Physics* (Butterworth-Heinemann, Oxford, 1994), Vol. 2.

[34] S. Yushanov, J. S. Crompton, and K. C. Koppenhoefer, " Mie scattering of electromagnetic waves," https://cn.comsol.com/paper/download/181101/crompton_paper.pdf.

[35] V. Asadchy, I. A. Faniayeu, Y. Radi, and S. A. Tretyakov, Photon. Nanostruct. Fund. Appl. **12**, 298 (2014).

[36] A. A. High, R. C. Devlin, M. P. Alan Dibos, D. S. Wild, J. Perczel, N. P. de Leon, M. D. Lukin, and H. Park, Nature (London) **522**, 192 (2015).

[37] D. Correas-Serrano and J. S. Gomez-Diaz, Phys. Rev. B **100**, 081410(R) (2019).

[38] Y. Yang, L. Jing, L. Shen, Z. Wang, B. Zheng, H. Wang, E. Li, N. Shen, T. Koschny, C. M. Soukoulis, and H. Chen, Npg Asia Mater. **9**, e428 (2017).

[39] S. B. Wang and C. T. Chan, Nat. Commun. **5**, 3307 (2014).

[40] N. K. Paul, D. Correas-Serrano, and J. S. Gomez-Diaz, Phys. Rev. B **99**, 121408(R) (2019).